

## Original article

# MicroRNA-322-5p promotes lipopolysaccharide-induced acute kidney injury mouse models and mouse primary proximal renal tubular epithelial cell injury by regulating T-box transcription factor 21/mitogen-activated protein kinase/extracellular signal-related kinase axis

Xiaobing Ji<sup>a</sup>, Xiaodong Liu<sup>b</sup>, Xiangxiang Li<sup>c</sup>, Xin Du<sup>a</sup>, Li Fan<sup>a,\*</sup>

<sup>a</sup> Department of Nephrology, Nanjing First Hospital, Nanjing Medical University, Nanjing 210006, Jiangsu, China

<sup>b</sup> Department of Nephrology, The Second People's Hospital of Lianyungang, Affiliated to Kangda College of Nanjing Medical University, Lianyungang 222023, Jiangsu, China

<sup>c</sup> Department of Nephrology, Nanjing Yuhua Hospital, Yuhua Branch of Nanjing First Hospital, Nanjing 210039, Jiangsu, China

## ARTICLE INFO

## Article history:

Received 15 November 2022

Accepted 25 January 2023

Available online 2 February 2023

## Keywords:

miR-322-5p

Acute kidney injury

Tbx21

MAPK/ERK signaling pathway

## ABSTRACT

**Introduction and objectives:** Acute kidney injury (AKI) is a common devastating complication characterized by an abrupt loss of renal function. It is of great significance to explore promising biomarkers for AKI treatment.

**Materials and methods:** Here, we established LPS (lipopolysaccharide)-induced AKI mice models and LPS-induced AKI mouse renal tubular epithelial cell model. The severity of AKI was determined by the levels of BUN (blood urea nitrogen) and SCr (serum creatinine), the observation of pathological section as well as the renal tubular injury score. The apoptosis was determined by the measurement of Caspase-3 and Caspase-9 activities, and cell apoptosis assays. qRT-PCR (quantitative real-time PCR) and western blot revealed that miR-322-5p (microRNA-322-5p) was up-regulated in LPS-induced AKI models while Tbx21 (T-box transcription factor 21) was down-regulated in LPS-induced AKI models. Dual-luciferase reporter and RNA pulldown assays detected the interaction of Tbx21 with miR-322-5p.

**Results:** We found that miR-322-5p was overtly over-expressed in the *in vitro* LPS-induced AKI model and promoted the apoptosis of AKI mouse renal tubular epithelial cells via inhibiting Tbx21, which suppressed the mitochondrial fission and cell apoptosis through MAPK/ERK (mitogen-activated protein kinase/extracellular signal-related kinase) pathway.

**Conclusions:** We demonstrated that miR-322-5p promotes LPS-induced mouse AKI by regulating Tbx21/MAPK/ERK axis, which might provide new sights for AKI research.

© 2023 Sociedad Española de Nefrología. Published by Elsevier España, S.L.U. This is an open access article under the CC BY-NC-ND license (<http://creativecommons.org/licenses/by-nc-nd/4.0/>).

\* Corresponding author.

E-mail address: [fanlisiyuan@163.com](mailto:fanlisiyuan@163.com) (L. Fan).

<https://doi.org/10.1016/j.nefro.2023.01.009>

0211-6995/© 2023 Sociedad Española de Nefrología. Published by Elsevier España, S.L.U. This is an open access article under the CC BY-NC-ND license (<http://creativecommons.org/licenses/by-nc-nd/4.0/>).

## MicroRNA-322-5p promueve en ratones los modelos de insuficiencia renal aguda inducidos por lipopolisacáridos y la lesión de las células epiteliales del túbulo renal proximal primario, mediante la regulación del eje factor 21 de transcripción de T-box / proteína quinasa activada por mitógenos/quinasa relacionada con la señal extracelular

### R E S U M E N

#### Palabras clave:

miR-322-5p  
Insuficiencia renal aguda  
Tbx21  
Vía de señalización de  
MAPK/ERK

**Introducción y objetivos:** La insuficiencia renal aguda (IRA) es una complicación común devastadora caracterizada por una pérdida abrupta de la función renal. Es de vital importancia explorar biomarcadores prometedores para el tratamiento de la IRA.

**Materiales y métodos:** Establecimos aquí un modelo de ratones con IRA inducido por lipopolisacáridos (LPS) y un modelo de células epiteliales del túbulo renal en ratones. La severidad de IRA fue determinada por los niveles de NUS (nitrógeno ureico en sangre) y SCr (creatinina sérica), la observación de la sección patológica, así como la puntuación del daño renal tubular. La apoptosis fue determinada mediante la medición de las actividades de Caspasa-3 y Caspasa-9, y los ensayos de apoptosis celular. Las pruebas qRT-PCR (PCR cuantitativa en tiempo real) y Western blot revelaron que miR-322-5p (microRNA-322-5p) se incrementaba en los modelos de IRA inducidos por LPS, mientras que Tbx21 (factor 21 de transcripción de T-box) disminuía en los modelos de IRA inducidos por LPS. Los ensayos del reportador de luciferasa dual y de precipitación pulldown de ARN detectaron la interacción entre Tbx21 y miR-322-5p.

**Resultados:** Encontramos que miR-322-5p se hallaba manifiestamente incrementado en el modelo in vitro de IRA inducido por LPS, y promovió la apoptosis de células epiteliales del túbulo renal de IRA en ratones mediante la inhibición de Tbx21, lo cual suprimió la fisión mitocondrial y la apoptosis a través de la vía MAPK/ERK (proteína quinasa activada por mitógeno/quinasa relacionada con la señal extracelular).

**Conclusiones:** Demostramos que miR-322-5p promueve la IRA inducida por LPS en ratones mediante la regulación del eje Tbx21/MAPK/ERK, lo cual podría aportar una percepción nueva para la investigación sobre la IRA.

© 2023 Sociedad Española de Nefrología. Publicado por Elsevier España, S.L.U. Este es un artículo Open Access bajo la licencia CC BY-NC-ND (<http://creativecommons.org/licenses/by-nc-nd/4.0/>).

## Introduction

Acute kidney injury (AKI) is a common complication, which is defined by a repaid loss of kidney function based on an increase in the levels of BUN (blood urea nitrogen) and SCr (serum creatinine).<sup>1</sup> This life-threatening complication results in two million deaths per year and may be caused by various clinical conditions.<sup>2</sup> The categories of AKIs conventionally include prerenal, intrarenal and postrenal causes.<sup>3</sup> There are no specific therapies which can attenuate AKI and promote recovery.<sup>4</sup> Renal replacement therapy and correcting reversible causes are main options of AKI treatment at present.<sup>3</sup> New diagnostic techniques (e.g., renal biomarkers) have the potential of assisting early diagnosis,<sup>3</sup> thus it is imperative to explore the potential biomarkers and investigate the underlying mechanism of AKI progression.

MiRNAs (microRNAs) are a class of small non-coding RNAs (ncRNAs) that can act as regulators of their target genes to involve in biological processes.<sup>5</sup> MiRNA dysregulation contributes to the development and progression of multiple diseases, including AKI.<sup>6</sup> Increasing evidence has proven the potential of miRNAs to act as new diagnostic biomarkers

of AKI,<sup>7</sup> such as miR-16,<sup>8</sup> miR-494<sup>9</sup> and miR-101.<sup>10</sup> Herein, we investigated the role of potential AKI-related miRNA in AKI. MiRNAs exerts their functions in human diseases usually through direct regulation of their downstream mRNAs (messenger RNAs).<sup>11–13</sup> In our current study, as miRNA–mRNA axis in AKI remains largely unknown, we also explored its downstream mRNA and its relevant regulatory mechanism in AKI.

The purpose of this research is to uncover potential AKI-related miRNA and the downstream mechanism. To obtain this aim, we established LPS (lipopolysaccharide)-induced AKI mice model and LPS-induced AKI mouse renal tubular epithelial cell model for the follow-up AKI-focused investigations. Then, we utilized the bioinformatics tool GEO (Gene Expression Omnibus) to screen out miR-322-5p and applied starBase to acquire its downstream target Tbx21, and then explored the impact of miR-322-5p/Tbx21 axis on cell apoptosis in LPS-induced AKI models. Given that MAPK/ERK (mitogen-activated protein kinase/extracellular signal-related kinase) pathway has been shown to be linked to cell apoptosis in multiple cancers,<sup>14,15</sup> we hypothesized this pathway was potentially involved in miR-322-5p/Tbx21 axis-regulated LPS-induced AKI.

## Materials and methods

### Cell culture

Mouse primary proximal renal tubular epithelial cells were procured from Cell Biologics, Inc. Following the manufacturer's manual, DMEM/F-12 (Dulbecco's Modified Eagle Medium/Nutrient Mixture F-12, Gibco-BRL, Carlsbad, CA, USA) was applied for cell culture, with the addition of 10% FBS (fetal bovine serum; Gibco-BRL). HEK-293T cells supplied by National Institute for the Control of Pharmaceutical and Biological Products (NICPBP) were cultured in DMEM (Gibco-BRL), supplemented with the medium supplements including 10% FBS and 1% Penicillin-Streptomycin Solution (Cat#: 15140122, Gibco-BRL).

### LPS-induced AKI mouse models *in vivo* and *in vitro*

A total of nine 5-week-old mice (female) supplied by Model Animal Institute of Nanjing University were treated with a standard laboratory diet. Animal experiments were approved by the Ethics Committee of the Nanjing First Hospital. LPS was dissolved into normal saline and used for intraperitoneal injection at 10 mg/kg for different time.<sup>16</sup> The kidney tissue and serum samples were collected at 0, 12 and 24 h. Here, LPS-induced AKI mice model was established after treatment with LPS for 24 h. To establish *in vitro* AKI cell model, we treated mouse primary renal tubular epithelial cells with LPS (0, 2.5, 5  $\mu$ g/mL) for different time.<sup>17</sup> Here, the mostly used *in vitro* AKI cell model was constructed with LPS treatment (5  $\mu$ g/mL) for 24 h.

### Renal function test

Renal function was evaluated by measuring the levels of BUN and SCr in LPS-induced AKI mice in line with the described protocol.<sup>18</sup> The former was detected using QuantiChrom™ Urea Assay Kit (BioAssay Systems) and the latter using QuantiChrom™ Creatinine Assay Kit (BioAssay Systems), following the protocols of the supplier.

### Assessment of renal oxidative stress levels

To assess oxidative stress in renal tissues of AKI mice after indicated LPS treatment, the levels of oxidative stress marker MDA (malondialdehyde) and antioxidant enzymes including CAT (catalase), SOD (superoxide dismutase) and GSH-Px (glutathione peroxidase) were detected via utilizing commercially available assay kits as per the supplier's directions. MDA level was detected utilizing assay kit supplied by Beijing Xinchengyuan Biomedical Technology Co., LTD. (Beijing, China); SOD and GSH-Px levels were detected by Invitrogen assay kit; CAT level was detected by Thermo Scientific assay kit (Rockford, IL, USA). The experiments were guided by the described protocol.<sup>18</sup>

**Table 1 – Sequences used for transfections.**

mimic-NC	uuguaagguucgacgacuuuaa
mimic-miR-322-5p	agguuuuguacuuacgacgac
inhibitor-NC	uaaguagucguguccucaa
inhibitor-miR-322-5p	gucgucguuaaguacaaaaccu

### Quantitative real-time PCR (qRT-PCR)

Total RNA was extracted from mouse primary proximal renal tubular epithelial cells and kidney tissue samples by using Trizol reagent (Takara, Japan). Reverse transcription and cDNA (complementary DNA) synthesis was implemented by using Hifair® III 1st Strand cDNA Synthesis SuperMix for qPCR (Cat#: 11141ES10, Takara, Japan) or miScript II RT Kit (Cat#: 218160, Qiagen, Hilden, Germany). qPCR was performed using qRT-PCR Kit (Cat#: QR0100-1KT, Sigma-Aldrich, St. Louis, MO, USA). Lastly, we calculated relative RNA levels as per the  $2^{-\Delta\Delta Ct}$  method.<sup>19</sup>

### Vector construction and cell transfection

Short hairpin RNAs (shRNAs) directly against Tbx21 (sh-Tbx21-1, sh-Tbx21-2, sh-Tbx21-3) and negative control of shRNA (sh-NC), pcDNA3.1 empty vector, and pcDNA3.1-Tbx21 were supplied by GenePharma (Shanghai, China). Cells were placed on the 6-well plates at a density of  $7 \times 10^5$  cells per well and incubated for 6 h followed by transfection with indicated plasmids using Lipofectamine 2000 (Cat#: 11668019, Invitrogen). MiR-322-5p mimics, miR-322-5p inhibitors, as well as their negative controls (mimic-NC and inhibitor-NC) were constructed by RiboBio (Guangzhou, China), and the sequences are listed in Table 1. Then, 250 pmol of miR mimics/inhibitors were transfected into cells incubated in a 6-well plate via Lipofectamine 2000 for 48 h.

### Western blot

Western blot was carried out as previously described.<sup>20</sup> Total proteins were isolated using Total Protein Extraction Kit (Cat#: PROTOT-1KT, Sigma-Aldrich) in line with the manufacturer's recommendations. In this assay, protein concentration was measured by Bradford Protein Assay Kit (Cat#: P0006C, Beyotime Biotechnology, Shanghai, China). The protein extracts were loaded onto SDS-PAGE (Cat#: P0670-250 mL, Beyotime Biotech, Shanghai, China), followed by protein transfer onto PVDF membranes (Sigma-Aldrich). The membranes were sealed with non-fat milk in TBST for 1 h at room temperature and subsequently incubated with primary antibodies at 4 °C overnight. After TBST washing, the membranes were subjected to 1 h of incubation with secondary antibodies, followed by TBST washing. Then, the membranes were incubated with ECL reagent (Absin, Shanghai, China) at room temperature and photographed. The antibodies used in this assay included Anti- $\beta$ -actin (Cat#: ab8227, Abcam, Cambridge, Mass, USA), Anti-ERK1 + ERK2 (phospho T202 + Y204; Cat#: ab223500, Abcam), and Anti-T-bet/Tbx21 (Cat#: ab91109, Abcam).  $\beta$ -Actin was used as an internal loading control. For each antibody, the experiment using each set of samples was performed in triplicate.

**Table 2 – The specific sequence of the 3'UTR region used in the luciferase experiments.**

Tbx 3'U TR-WT	<p>GAAAATGCCGCTGAATTGGAAGGTGCCCACTAACTTAGAAAAACAGACGCGGG  GCTGAGAGCCCCGAGCTCTTCCCCATCCCTTCCCTGTATAGTGATTGGTTGGAG  AGGAAGCGGGGCAAGAAGGATCTGGGGTTTACTTCTTGTTCCTGGCCCCACA AGGAAA  TACGACAGGAGTGTCCCTGCCCTTCTCTGCCCGAACTACAGTCA  CGA . CCTGGTGTCTTCTGACCCCATGGTTCATGGAGAACGGAGAATGGAC  TCCAGAGAGTTTGGACCCAGAGGGACTTCATGGCTTCTGCGAGGTGGAGGG  GTCGGGGTGGGGAGTCCAGGAGAGCTGCTCTTCCCTGTCCAGTCAGTAAC  TTTCAACTGTGGTCTGACACCTGTGTTAATCTCTGACCTGAAAAGTGAAGATA  CACGCATTTTACAACAGCCAGCCAAACAGAGAAGACTCAGGTGACTGCGGG  CGGACTGGGCCACCTGCGAGGAGACAAGAGGGTGGGTGCAGAGGAAGGGT  TTGAAGGGTGCACATTTACCAGGCGAGGTCACTTGAACCGGTGTGTACACA <u>CACGGGTGTCTCIIIIIIIA</u>  <u>TTTCTTCGGGAGGGGGAGGCTATTATTGTAGAG</u>  AGTGGTGTCTGGATGATTTCTTCTGTTTTCATCACTTTCTGGAATAAACAT GGACCTGGTAAA</p>
Tbx 3'U TR-Mut	<p>GAAAATGCCGCTGAATTGGAAGGTGCCCACTAACTTAGAAAAACAGACGCGGG  GCTGAGAGCCCCGAGCTCTTCCCCATCCCTTCCCTGTATAGTGATTGGTTGGAG  AGGAAGCGGGGCAAGAAGGATCTGGGGTTTACTTCTTGTTCCTGGCCCCACA AGGAAA  TACGACAGGAGTGTCCCTGCCCTTCTCTGCCCGAACTACAGTGT  CGTTGCACGACGACGATCTGACCCCATGGTTCATGGAGAACGGAGAATGGA  CTCCAGAGAGTTTGGACCCAGAGGACTTCATGGCTTCTGCGAGGTGGAGG  GGTCGGGGTGGGGAGTCCAGGAGAGCTGCTCTTCCCTGTCCAGTCAGTAA  CTTTCAACTGTGGTCTGACACCTGTGTTAATCTCTGACCTGAAAAGTGAAGAT  ACACGCATTTTACAACAGCCAGCCAAACAGAGAAGACTCAGGTGACTGCGG  GCGGACTGGGCCACCTGCGAGGAGACAAGAGGGTGGGTGCAGAGGAAGGG  TTTGAAGGGTGCACATTTACCAGGCGAGGTCACTTGAACCGGTGTGTACAC  <u>ACACGGGTGTCTC111111</u> <u>ATTTCTTCGGGAGGGGGAGGCTATTATTGTAG</u>  GAGTGGTGTCTGGATGATTTCTTCTGTTTTCATCACTTTCTGGAATAAACAT TGGACCTGGTAAA</p>

### Measurement of Caspase-3 and Caspase-9 activity

The experiments were conducted as described.<sup>21</sup> According to the supplier's recommendations, the activity of Caspase-3 or Caspase-9 in cell lysates was detected using Caspase-3 Colorimetric Assay Kit (KeyGEN Biotech, Nanjing, China) or Caspase-9 Colorimetric Assay Kit (KeyGEN Biotech), respectively.

### Dual luciferase reporter assay

Dual luciferase reporter assay was performed as previously described.<sup>22</sup> The pmirGLO vectors were purchased from Promega (Madison, WI, USA). Utilizing Lipofectamine 2000, luciferase reporter vectors (pmirGLO, pmirGLO-Tbx21 3'UTR-WT or pmirGLO-Tbx21 3'UTR-Mut) were co-transfected with 5 pmol of NC mimic or miR-322-5p mimic (20  $\mu$ M) into cells. 48 h later, relative luciferase activities were detected with Dual-Luciferase<sup>®</sup> Reporter Assay System (Promega). The sequences for Tbx21 3'UTR are listed in [Table 2](#).

### RNA pull-down assay

RNA pull-down assay was implemented as previously described.<sup>23</sup> The biotin-labeled probes (including Bio-NC, Bio-Tbx21-WT, and Bio-Tbx21-Mut) was obtained from RiboBio. Later, Cell lysates were mixed with indicated probes overnight, and then subjected to incubation with streptavidin-coated magnetic beads (Sigma-Aldrich) for 2 h at 4 °C. The biotinylated RNA complexes were pulled down and the enrichment of RNA was measured via qRT-PCR.

### Terminal-deoxynucleotidyl transferase mediated nick end labeling (TUNEL)

TUNEL assay was conducted for the evaluation of cell apoptosis as previously described.<sup>24</sup> The transfected cells underwent 15 min of fixation in 4% paraformaldehyde at room temperature. *In situ* Cell Death Detection Kit (Roche, Mannheim, Germany) was used to perform TUNEL staining as per the supplier's manual. Lastly, TUNEL-positive cells were counted under a fluorescence microscope (Cat#: XSP-63B, Shanghai Optical Instrument Factory No.1).

### Flow cytometry apoptotic analysis

Flow cytometry analysis was implemented to test cell apoptosis as previously described.<sup>25</sup> After incubation, the cells were collected and dyed by Annexin V-FITC/PI from BD Biosciences (San Diego, CA, USA), followed by analysis with BD Flow Cytometer (BD Biosciences, Franklin Lakes, NJ, USA) analysis.

### PAS (Periodic Acid-Schiff) staining

PAS staining was implemented as previously described.<sup>26</sup> The section of LPS-treated mice's kidney tissue samples was stained using PAS (Cat#: Ab150680, Abcam). Pathological section was reviewed under a confocal microscope (Smartzoom 5, Zeiss, Shanghai, China).

### Histological analysis

The renal tubular injury was characterized with deformation of vacuoles, loss of brush border, kidney tubular dilation or nuclear condensation. The severity of tubular injury

was scored as per the following scoring system: 0 to 4 based on the percentage of the injured area of the section (0=no change; 1=changes affecting <25%; 2=changes affecting 25–50%; 3=changes affecting 50–75%; 4=changes affecting >75% of the section). At least six different visual fields were randomly chosen under a confocal microscope (magnification,  $\times 400$ ; Smartzoom 5, Zeiss) and the average score was calculated.

### Observation of mitochondrial morphology

Mitochondrial morphology was detected with the help of Mitotracker Red CMXRos (Invitrogen) as per the previous protocol.<sup>27</sup> Mitochondrial branch length was observed by the inverted microscope (Nikon Ti-E, Nikon Corporation) and the mean branch length was measured by ImageJ.

### U0126 treatment

U0126 served as the inhibitor of MAPK/ERK signaling pathway.<sup>28</sup> U0126 (Cat#: HY-12031, Med Chem Express, Monmouth Junction, NJ, USA) treatment was performed as per the manual of the supplier.

### Statistical analysis

Bio-repeats in each experiment were implemented in triplicate and technical replicates were repeated three times for each bio-repeat. Data analysis was processed with the application of SPSS 22.0 (SPSS Inc., Chicago, IL, USA). The experimental data were presented as mean  $\pm$  SD (standard deviation). In this study, group difference was analyzed by Student's t-test, one-way ANOVA (analysis of variance) or two-way ANOVA, followed by Dunnett or Tukey correction. *P* value less than 0.05 indicated data were statistically significant.

## Results

In this research, we established LPS-induced AKI *in vitro* model and *in vivo* model for the following investigations to explore the underlying mechanism of AKI. Bioinformatics tools and experiments were utilized to determine the object of research (miRNA of interest: miR-322-5p) and its downstream target (Tbx21). We then performed TUNEL staining and detected the activity of apoptotic markers (Caspase-3 and Caspase-9) to evaluate the impact of miR-322-5p on cell apoptosis in LPS-induced AKI model. Given that stimulation of MAPK/ERK signaling pathway is linked to cell apoptosis, we further probed into whether it was involved in the process of miR-322-5p/Tbx21 axis affecting the apoptosis of *in vitro* AKI model.

### Establishment of LPS-induced AKI mice model and mouse renal tubular epithelial cell model

Given that the levels of BUN and SCr represent the severity of AKI, we firstly measured the levels of BUN and SCr in LPS-treated mice. The results showed that both serum BUN and SCr levels in LPS-treated mice markedly were elevated as the time of LPS treatment went by (Fig. 1A, B; \**P* < 0.05, \*\**P* < 0.01).

Then, we observed swollen renal tubular epithelial cells, deformed vacuoles, and abnormally narrowed renal tubules in the pathological section of LPS-treated mice's kidney tissues and found that the symptoms were getting worse as time went by (Fig. 1C), which suggested the increasing severity of AKI. LPS treatment exacerbated renal tubular injury in LPS-treated mice (Fig. 1D; \*\**P* < 0.01). Consistent with this, we also observed that the level of oxidative stress in AKI mice renal was increased with LPS treatment time, since LPS increased the level of MDA and reduced the activities of SOD, CAT and GSH-Px in a time-dependent manner (Fig. S1A–D; \*\**P* < 0.01). In addition, we assessed the activity of apoptotic markers, including Caspase-3 and Caspase-9. The results demonstrated that both Caspase-3 activity and Caspase-9 activity in renal tubular cells of LPS-treated mice were significantly enhanced as the time of LPS treatment (Fig. 1E, F; \**P* < 0.05, \*\**P* < 0.01). Meanwhile, we also detected that the levels of caspase-3, caspase-9 and Bax were elevated whereas the level of Bcl-2 was reduced in renal tissues from AKI mice along with the increasing LPS treatment dose (Fig. S1E). Moreover, we observed that TUNEL-positive cells in LPS-treated mice's kidney tissues were greatly increased as well (Fig. 1G, H; \*\**P* < 0.01). Together, we confirmed that LPS-induced AKI mice model was established successfully. Given that the highest efficiency of 24-h LPS treatment, we chose it for *in vivo* experiments in this research.

Next, we measured the apoptosis rate of LPS-treated mouse renal tubular epithelial cells. The apoptosis rate showed an obvious increase in a time-dependent manner (Fig. 1I; \*\**P* < 0.01). Meanwhile, Caspase-3 and Caspase-9 activities were enhanced by LPS treatment (Fig. 1J, K; \**P* < 0.05, \*\**P* < 0.01). Thereby, we confirmed the successful establishment of *in vitro* AKI cell model. Since 24 h of LPS treatment presented the higher efficiency than 12-h LPS treatment, we chose it for *in vitro* experiments in this research.

### miR-322-5p promotes the apoptosis of AKI renal tubular epithelial cells

We next explored a functional miRNA in AKI. With the application of GSE130796 (screening condition: log<sub>2</sub> | FC | > 1.0, Padj < 0.05), we obtained five putative miRNAs (miR-122-5p, miR-126a-5p, miR-322-5p, miR-200a-5p, and miR-374-5p). Then qRT-PCR detected that both miR-126a-5p and miR-322-5p were elevated by LPS treatment at 24 h in AKI renal tubular epithelial cells (Fig. 2A, \*\**P* < 0.01). Further, we explored whether the expression of miR-126a-5p and miR-322-5p was affected by LPS in a dose- or time-dependent manner. As illustrated in Fig. 2B (\**P* < 0.05, \*\**P* < 0.01), the expression level of miR-322-5p, instead of miR-126a-5p, was heightened with the treating time of LPS in AKI mice renal tissues. Likewise, the results in AKI cell model were consistent with those in *in vivo* model (Fig. 2C, D; \**P* < 0.05, \*\**P* < 0.01). Therefore, we speculated that miR-322-5p might be able to regulate the apoptosis of AKI renal tubular epithelial cells.

We then evaluated the regulatory role of miR-322-5p on the apoptosis of AKI renal tubular epithelial cells. The effect of miR-322-5p overexpression or deficiency on the apoptosis rate of AKI renal tubular epithelial cells was identified by flow cytometry apoptotic analysis. The results displayed

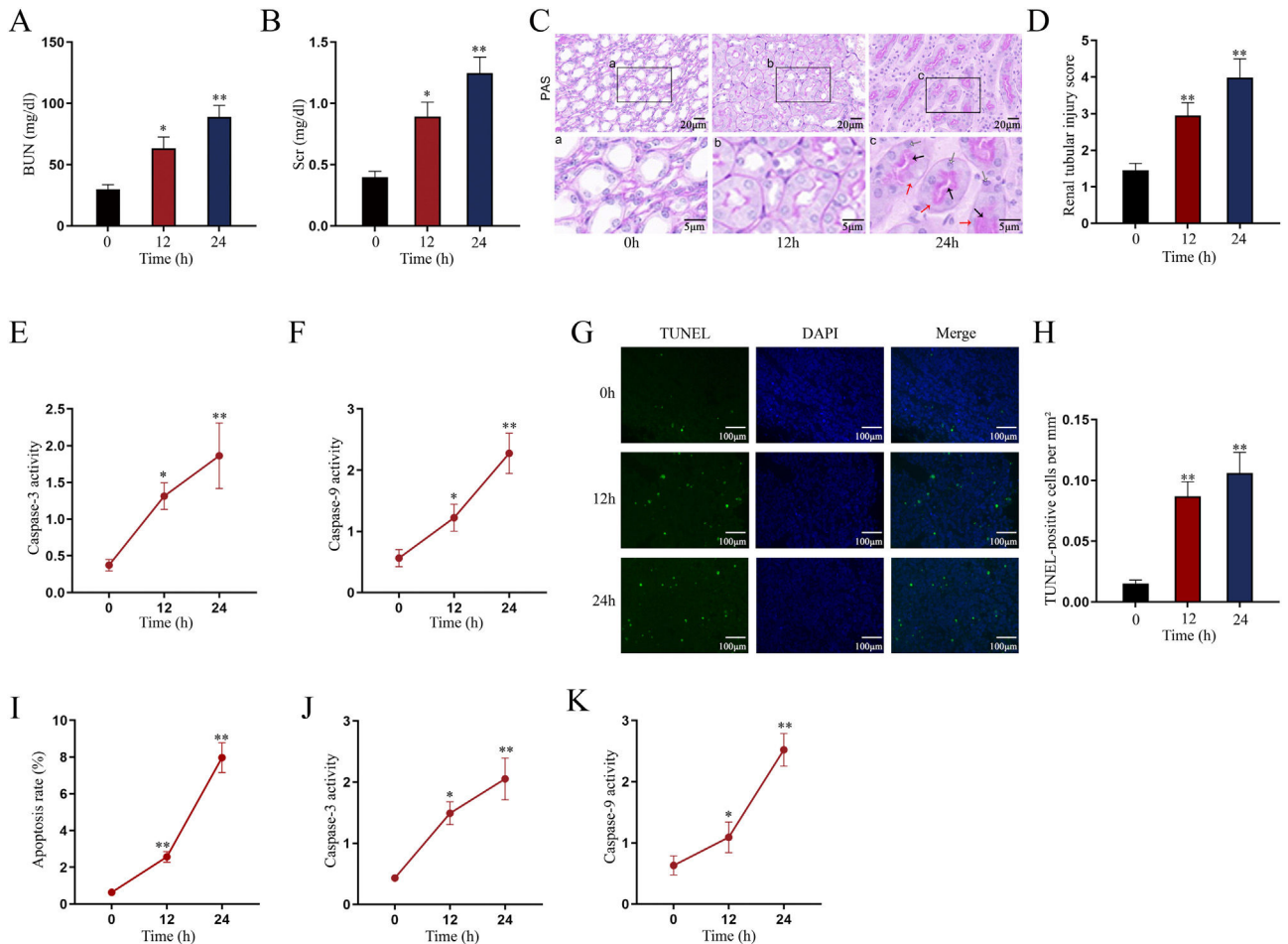


**Fig. 1** – Establishment of LPS-induced AKI mice model and mouse renal tubular epithelial cell model. For LPS-induced AKI mice model, mice were intraperitoneally injected with LPS (10 mg/kg) for 0, 12, and 24 h. (A, B) The BUN and SCr levels were examined via qRT-PCR analysis (one-way ANOVA, Tukey). (C) The images of pathological section of LPS-treated mouse kidney tissue samples stained by PAS were shown (scale bar: upper: 20  $\mu$ m, lower: 5  $\mu$ m). Red arrows indicate swelling of renal tubular epithelial cells; black arrows indicate tubular lumen shrinkage; white arrows indicate vacuolar deformation. (D) The LPS-treated mice model's renal tubular injury score was marked ranging from 0 to 4: 0 (no change); 1 (changes affecting < 25%); 2 (changes affecting 25–50%); 3 (changes affecting 50–75%); 4 (changes affecting > 75%) (one-way ANOVA, Tukey). (E, F) The activity of Caspase-3 and Caspase-9 of renal tubular cell in LPS-induced AKI mice model was shown (one-way ANOVA, Tukey). (G) The apoptosis of LPS-treated mice's kidney tissue section was determined by TUNEL assay. (H) The TUNEL-positive cells were measured in the LPS-treated mouse renal tubular epithelial cell model at different time points (one-way ANOVA, Tukey). (I) For LPS-treated mouse renal tubular epithelial cell model, cells were treated with LPS (5  $\mu$ g/mL) for 0, 12, and 24 h. The apoptosis rate of *in vitro* LPS-induced AKI model was increased as time went by (one-way ANOVA, Tukey). (J, K) Caspase-3 and Caspase-9 activities were determined in LPS-treated mouse renal tubular epithelial cell model (one-way ANOVA, Tukey). \*\* $P < 0.01$ , \* $P < 0.05$ .

that up-regulation of miR-322-5p increased the apoptosis rate while knockdown of miR-322-5p exhibited the opposite effect (Fig. 2E, F; \*\* $P < 0.01$ ), indicating that miR-322-5p promotes the apoptosis of AKI renal tubular epithelial cells. Additionally, we measured the impact of miR-322-5p on the activity of apoptotic markers. The results showed that elevation of miR-322-5p enhanced caspase-3 activity while inhibition of miR-322-5p decreased caspase-3 activity (Fig. 2G, H; \*\* $P < 0.01$ ). Also, the caspase-9 activity was promoted by elevation of miR-322-5p but suppressed by ablation of miR-322-5p (Fig. 2I, J; \*\* $P < 0.01$ ). Taken together, miR-322-5p accelerates the apoptosis of AKI renal tubular epithelial cells.

### miR-322-5p promotes the apoptosis of AKI renal tubular epithelial cells via inhibiting *Tbx21*

Moreover, we probed into the molecular mechanism of miR-322-5p in AKI renal tubular epithelial cells. Previous literatures have reported that miRNAs play a role in regulating target gene expression.<sup>29</sup> Through the preliminary prediction on the starBase website (<http://starbase.sysu.edu.cn/>), we selected six putative mRNAs associated with cell proliferation, morphology, and apoptosis in cancers, including Grb2,<sup>30</sup> Rictor,<sup>31</sup> *Tbx21*,<sup>32</sup> *Ddx3x*,<sup>33</sup> *Ube4b*,<sup>34</sup> and *Vegfa*<sup>35</sup> (Fig. 3A). Subsequently, we measured the expression levels of above

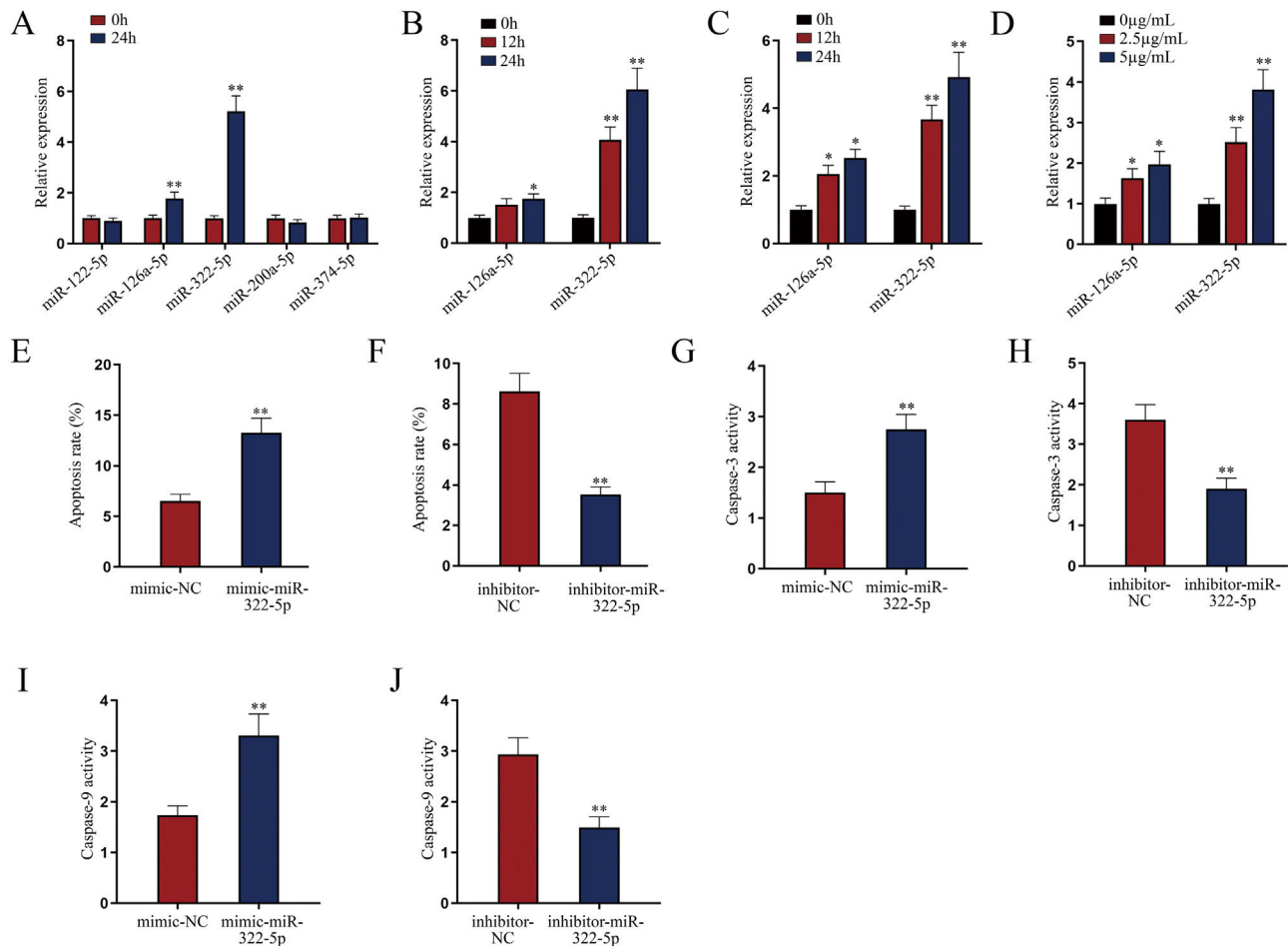


**Fig. 2 – miR-322-5p promotes the apoptosis of AKI renal tubular epithelial cells. (A)** Relative expression levels of putative miRNAs in LPS-treated mouse renal tubular epithelial cell model (5  $\mu\text{g}/\text{mL}$ ; 24 h) were detected via qRT-PCR (Student's *t*-test). **(B)** The expression levels of miR-126a-5p and miR-322-5p in renal tubular cells of AKI mice models were measured via qRT-PCR in mice under LPS treatment for different time (one-way ANOVA, Tukey). **(C, D)** The expression levels of miR-126a-5p and miR-322-5p were measured in mouse renal tubular epithelial cells under LPS treatment at the same dose of 5  $\mu\text{g}/\text{mL}$  for different time or with different doses for 24 h (one-way ANOVA, Tukey). **(E, F)** The apoptosis rate was increased by miR-322-5p mimic and decreased by miR-322-5p inhibitor (Student's *t*-test). **(G, H)** Caspase-3 activity was promoted by miR-322-5p and was inhibited by miR-322-5p inhibitor (Student's *t*-test). **(I, J)** Caspase-9 activity was enhanced by miR-322-5p and was repressed by miR-322-5p inhibitor (Student's *t*-test). The experiments as shown in (E–J) were performed in LPS-induced AKI mouse renal tubular epithelial cell model (5  $\mu\text{g}/\text{mL}$ ; 24 h). \*\**P* < 0.01, \**P* < 0.05.

candidate mRNAs in renal tubular cells of LPS-induced AKI mice model (10 mg/kg) and in LPS-induced AKI renal tubular epithelial cell model (5  $\mu\text{g}/\text{mL}$ ). The results showed that Tbx21 was significantly down-regulated in both LPS-induced AKI *in vivo* and *in vitro* models (Fig. 3B; \*\**P* < 0.01). Tbx21 were thereby selected for the subsequent investigations. To explore the effect of miR-322-5p on Tbx21 expression, we measured the mRNA level and protein level of Tbx21 under miR-322-5p mimic/inhibitor treatment. Tbx21 levels were visibly decreased by up-regulation of miR-322-5p (Fig. 3C, D; \*\**P* < 0.01), whereas those of Tbx21 were obviously increased by miR-322-5p silencing (Fig. 3E, F; \*\**P* < 0.01), indicating that miR-322-5p negatively modulates Tbx21 expression.

Besides, we investigated the effect of Tbx21 on the apoptosis of AKI renal tubular epithelial cells. The interference efficiency and overexpression efficiency of Tbx21 were

elucidated by qRT-PCR analysis. In view of the higher knock-down efficiency of sh-Tbx21-1 and sh-Tbx21-2 plasmids (Fig. 3G; \*\**P* < 0.01), we chose sh-Tbx21-1 and sh-Tbx21-2 for the following experiments; overexpression of Tbx21 was confirmed as qRT-PCR detected a significant increase in Tbx21 level in transfected cells with pcDNA3.1-Tbx21 (Fig. 3H; \*\**P* < 0.01). Through apoptosis assays, we found that depletion of Tbx21 significantly enhanced the apoptosis rate of LPS-induced AKI renal tubular epithelial cell model while overexpression of Tbx21 led to the reverse results (Fig. 3I, J; \*\**P* < 0.01). Likewise, Caspase-3 and Caspase-9 activities were strengthened by Tbx21 silencing but impaired by Tbx21 overexpression (Fig. 3K–N; \*\**P* < 0.01). Altogether, Tbx21 negatively modulates cell apoptosis in AKI renal tubular epithelial cells.

To further explore the physical interaction of miR-322-5p and Tbx21, we performed luciferase reporter and RNA

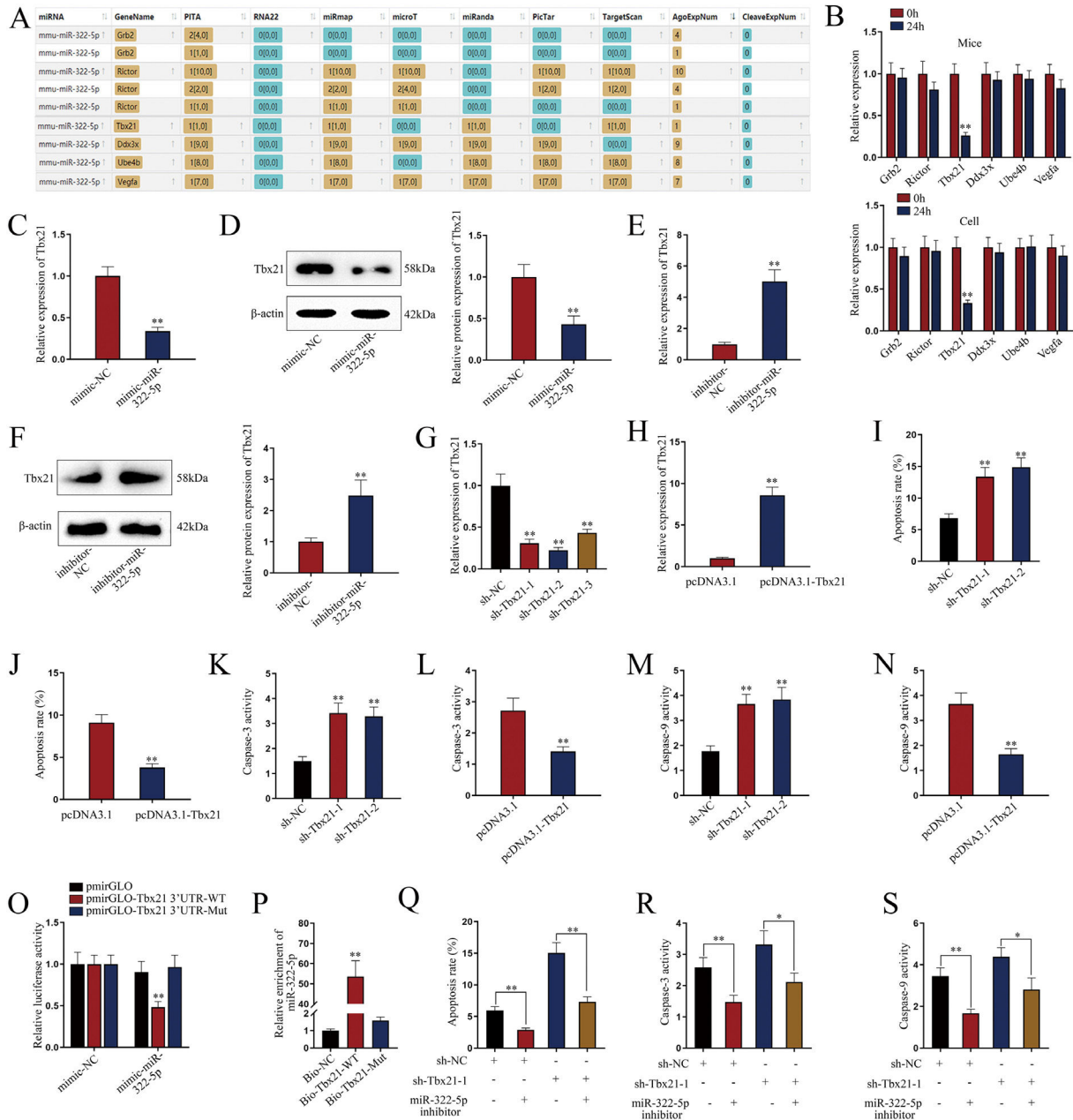


**Fig. 3 – miR-322-5p promotes the apoptosis of AKI renal tubular epithelial cells by targeting Tbx21.** (A) Six candidate downstream mRNAs of miR-322-5p were screened out by starBase (<http://starbase.sysu.edu.cn/>). (B) The expression levels of six mRNAs were detected in renal tubular cells of LPS-induced AKI mice model (10 mg/kg; 24h) and LPS-induced AKI mouse renal tubular epithelial cell model (5  $\mu$ g/mL; 24h) (Student's t-test). (C) qRT-PCR tested that Tbx21 mRNA level was reduced under miR-322-5p mimic treatment (Student's t-test). (D) Western blot revealed that the protein level of Tbx21 was lowered under miR-322-5p mimic treatment (Student's t-test). (E, F) Tbx21 mRNA and protein level under miR-322-5p inhibition were tested by qRT-PCR and western blot, respectively. Student's t-test. (G, H) The knockdown efficiency and overexpression efficiency of Tbx21 were verified by qRT-PCR analysis (one-way ANOVA, Tukey; Student's t-test). (I) The apoptosis rate was increased by Tbx21 knockdown (one-way ANOVA, Dunnett). (J) The apoptosis rate was decreased by Tbx21 overexpression (Student's t-test). (K, L) Caspase-3 activity was measured responding to Tbx21 knockdown (one-way ANOVA, Dunnett) and Tbx21 up-regulation (Student's t-test). (M, N) Caspase-9 activity was measured in cells with Tbx21 knockdown (one-way ANOVA, Dunnett) or overexpression (Student's t-test). (O) The luciferase activity was promoted by miR-322-5p overexpression in pmirGLO-Tbx21 3'UTR-WT group (two-way ANOVA, Tukey). (P) miR-322-5p was relatively enriched in Bio-Tbx21-WT group (one-way ANOVA, Tukey). (Q-S) Tbx21 deficiency could weaken the repressive effect of miR-322-5p inhibition on the apoptosis via measuring the apoptosis rate, Caspase-3 and Caspase-9 activities, respectively (one-way ANOVA, Tukey). The experiments as shown in C-S were performed in LPS-induced AKI mouse renal tubular epithelial cell model (5  $\mu$ g/mL; 24h). \*\* $P < 0.01$ , \* $P < 0.05$ .

pull-down assays in LPS-induced AKI mouse renal tubular epithelial cell model. As shown in Fig. 3O (\*\* $P < 0.01$ ), the luciferase activity of pmirGLO-Tbx21 3'UTR-WT was dramatically inhibited by miR-322-5p mimic while that of pmirGLO-Tbx21 3'UTR-Mut had no obvious change, suggesting that miR-322-5p could bind to Tbx21. The results of RNA pull-down assays also verified the same finding since miR-322-5p was overtly abundant in Bio-Tbx21-WT group instead of mutated group (Fig. 3P; \*\* $P < 0.01$ ). Rescue experiments were subsequently carried out to determine the impact of miR-322-5p/Tbx21 axis on cell apoptosis in AKI cell model. We found that Tbx21 knockdown attenuated the suppressive effect of downregulated miR-322-5p on the apoptosis rate of AKI renal tubular epithelial cells (Fig. 3Q; \*\* $P < 0.01$ ). In the meantime, silenced Tbx21 impaired the repression of miR-322-5p knockdown on the Caspase-3 activity and Caspase-9 activity as depicted in Fig. 3R and S (\* $P < 0.05$ , \*\* $P < 0.01$ ). In conclusion, miR-322-5p enhances the apoptosis of AKI renal tubular epithelial cells via negatively modulating Tbx21.

#### *Tbx21 modulates mitochondrial fission and cell apoptosis through MAPK/ERK signaling pathway*

As MAPK/ERK pathway has been reported to be associated with cell apoptosis,<sup>14,15</sup> we next investigated whether Tbx21 affects the MAPK/ERK signaling pathway. Western blots showed that the protein level of p-ERK1/2 and p-MAPK was increased after 24 h of LPS treatment (Fig. 4A; \*\* $P < 0.01$ ), implying the activation of MAPK/ERK signaling pathway in renal tubular cell of LPS-induced AKI mice model. As shown in Fig. 4B, p-ERK1/2 also showed a higher protein level after 24 h of LPS treatment (\* $P < 0.05$ , \*\* $P < 0.01$ ), displaying the stimulation of MAPK/ERK signaling pathway in LPS-induced AKI renal tubular epithelial cell model. Later, we explored the impact of Tbx21 on the MAPK/ERK signaling pathway. The results of western blot suggested that Tbx21 deficiency obviously increased p-ERK1/2 protein level (Fig. 4C; \* $P < 0.05$ , \*\* $P < 0.01$ ). Simultaneously, overexpression of Tbx21 largely reduced the protein level of p-ERK1/2 (Fig. 4D; \*\* $P < 0.01$ ). In a word, Tbx21 could impede the stimulation of MAPK/ERK pathway in LPS-induced AKI mice model and cell model.

Since the association between mitochondrial fission and cell apoptosis has been reported in previous studies,<sup>36,37</sup> we then investigated the effect of Tbx21 on mitochondrial morphology. Before that, we analyzed the mitochondrial morphology in LPS-induced AKI cell model. The mitochondria got rounded, small and fragmented upon LPS treatment (Fig. 4E), suggesting that the mitochondria were injured in LPS-induced AKI cell model. The mean branch length of mitochondria was significantly decreased caused by LPS treatment (Fig. 4F; \* $P < 0.05$ , \*\* $P < 0.01$ ), exhibiting the improved degree of mitochondrial fission. Next, we observed the mitochondrial morphology and found that upon ablation of Tbx21, the mitochondria got rounded, small and fragmented and the mean branch length was decreased (Fig. 4G, H; \*\* $P < 0.01$ ). On the contrary, the mitochondria became tubular and the mean branch length was increased upon up-regulation of Tbx21 (Fig. 4I, J; \*\* $P < 0.01$ ). The above results verified that Tbx21 suppresses mitochondrial fission in LPS-induced AKI renal tubular epithelial cell model. Afterwards, we used the inhibitor of

MAPK/ERK pathway U0126<sup>28</sup> to further verify whether Tbx21 affects mitochondrial fission through the MAPK/ERK pathway. The mitochondria became tabulated under U0126 treatment compared to sh-Tbx21-1 group (Fig. 4K). The measurement results of the mean branch length also verified the same finding as the mean branch length was relatively increased in sh-Tbx21-1 + U0126 group compared to that in sh-Tbx21-1 group (Fig. 4L; \* $P < 0.05$ , \*\* $P < 0.01$ ). To sum up, Tbx21 negatively regulates mitochondrial fission via MAPK/ERK signaling pathway.

Moreover, we detected the apoptosis rate of AKI mouse renal tubular epithelial cell model with indicated transfections. The data exhibited that the apoptosis rate was lower in sh-Tbx21-1 + U0126 group compared to that in sh-Tbx21-1 group (Fig. 4M; \*\* $P < 0.01$ ). Additionally, Caspase-3 and Caspase-9 activities were lowered in sh-Tbx21-1 + U0126 group compared to that in sh-Tbx21-1 group (Fig. 4N, O; \* $P < 0.05$ , \*\* $P < 0.01$ ). Thus, we concluded that Tbx21 negatively modulates mitochondrial fission and cell apoptosis via MAPK/ERK signaling pathway.

## Discussion

AKI is a common and serious problem threatening millions per year, resulting in deaths and disability.<sup>38</sup> Previous studies have confirmed the correlation between miRNAs and AKI.<sup>39</sup> For instance, miR-668 down-regulates MTP18 to preserve mitochondrial dynamics in IAKI (ischemic acute kidney injury).<sup>40</sup> miR-214 ameliorates AKI by impairing apoptosis via targeting DKK3 and stimulating the Wnt/ $\beta$ -catenin pathway.<sup>41</sup> In our study, we found a novel functional miRNA in AKI. Herein, we identified that miR-322-5p expression was increased in LPS-induced AKI model in time- and dose-dependent manner. More importantly, we found that miR-322-5p promotes the apoptosis of AKI renal tubule epithelial cells.

Besides, we uncovered the regulation mechanism of miR-322-5p in AKI. Given that miRNAs could modulate target gene expression,<sup>42</sup> we investigated potential miR-322-5p target in this research. Previous studies have identified several targets of miR-322-5p, such as Smad7,<sup>43</sup> IGF-1,<sup>44</sup> TSPAN5,<sup>45</sup> etc. Here, we presented a novel downstream target gene of miR-322-5p, Tbx21. Tbx21 has been proven to be a suppressor of MAPK/ERK signaling pathway in thyroid cancer.<sup>46</sup> Stimulation of MAPK/ERK signaling pathway is linked to cell apoptosis. For example, miR-497 promotes apoptosis through negative regulation of RAF-1-mediated MAPK/ERK signaling pathway.<sup>47</sup> Based on this, we speculated that miR-322-5p promotes the apoptosis via repressing Tbx21, which might inactivate the MAPK/ERK signaling pathway in AKI. Through the loss-of-function and gain-of-function experiments, we identified the inhibitory effect of Tbx21 on cell apoptosis in AKI models. We also manifested the mechanism by which Tbx21 regulated cell apoptosis in AKI through MAPK/ERK pathway. In this study, we demonstrated that Tbx21 inactivates MAPK/ERK signaling pathway in AKI.

Mitochondria are highly dynamic organelles undergoing regular fission and fusion cycles.<sup>48</sup> Mitochondrial fission is related to apoptosis and often occurs in AKI.<sup>36</sup> Alterations in mitochondrial morphology are related to changes

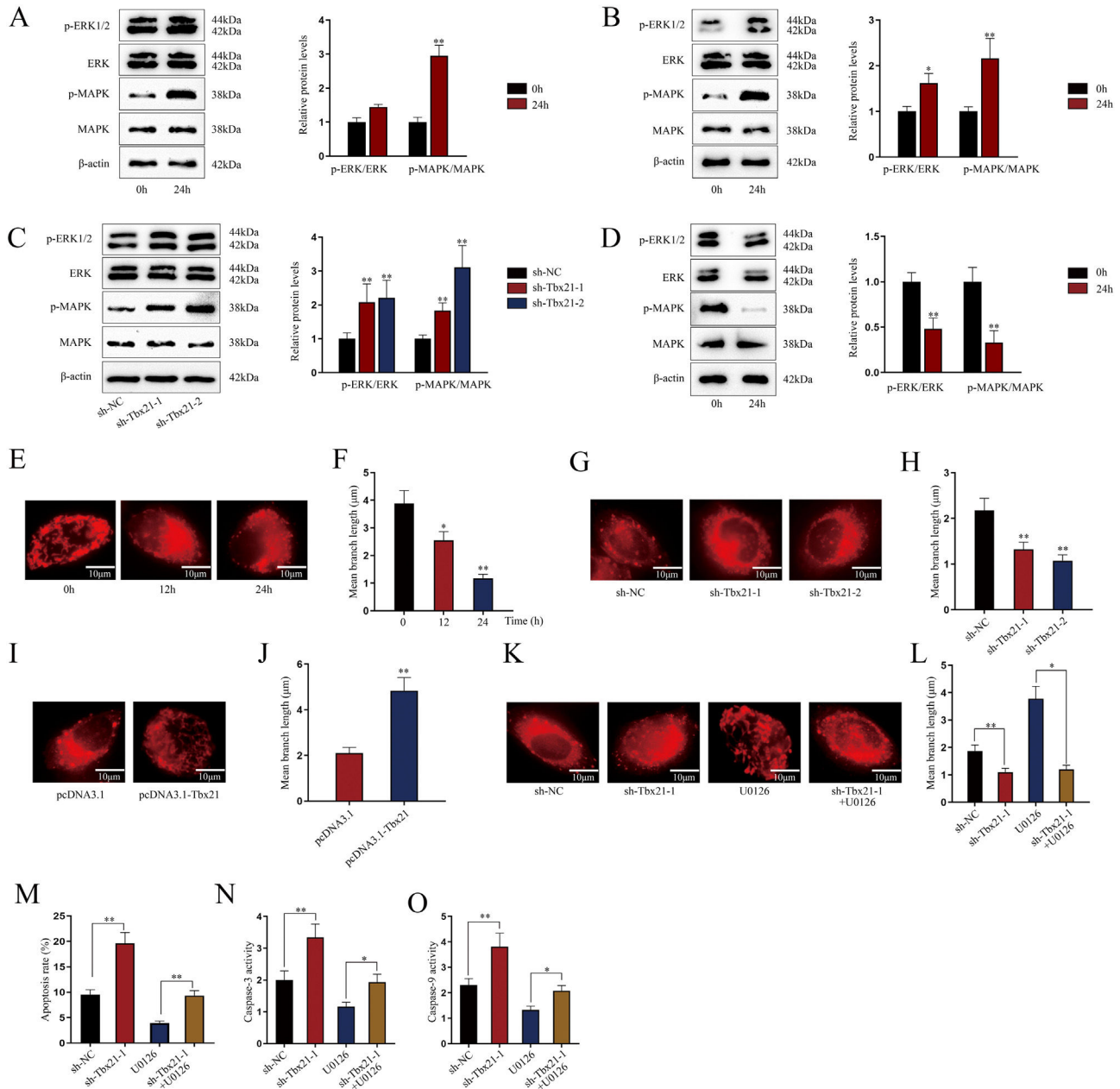


**Fig. 4 – Tbx21 modulates mitochondrial fission and cell apoptosis through MAPK/ERK signaling pathway. (A, B)** The protein level of p-ERK1/2 was increased in renal tubular cell of LPS-induced AKI mice model (10 mg/kg; 24 h) and LPS-induced AKI mouse renal tubular epithelial cell model (5 µg/mL; 24 h), individually (Student's *t*-test). **(C, D)** The protein level of p-ERK1/2 was increased by Tbx21 knockdown (one-way ANOVA, Dunnett) and was decreased by overexpressed Tbx21 in LPS-induced AKI mouse renal tubular epithelial cell model (5 µg/mL; 24 h) (Student's *t*-test). **(E)** The mitochondria became rounded, small and fragmented in LPS-treated mouse renal tubular epithelial cell model (5 µg/mL; 24 h). Scale bar = 10 µm. **(F)** The mean branch length was reduced in LPS-treated mouse renal tubular epithelial cell model (5 µg/mL; 0, 12, 24 h) (one-way ANOVA, Tukey). **(G)** The mitochondria became rounded, small and fragmented after down-regulating Tbx21. Scale bar = 10 µm. **(H)** The mean branch length was reduced after Tbx21 knockdown (one-way ANOVA, Tukey). **(I)** The mitochondria became tabulated after overexpressing Tbx21. Scale bar = 10 µm. **(J)** The mean branch length was increased after down-regulation of Tbx21 (Student's *t*-test). **(K–O)** U0126 treatment was used to inhibit the activity of MAPK/ERK signaling pathway. The inhibition of this pathway weakened the promoting effect of Tbx21 knockdown on the apoptosis via observing the mitochondrial morphology and measuring the mitochondrial mean branch length, the apoptosis rate, Caspase-3 and Caspase-9 activities, respectively (one-way ANOVA, Tukey). Scale bar = 10 µm. The experiments as shown in (G–O) were performed in LPS-induced AKI mouse renal tubular epithelial cell model (5 µg/mL; 24 h). \*\**P* < 0.01, \**P* < 0.05.

in metabolism, cell death and cell development.<sup>49</sup> In addition, previous studies have highlighted the therapeutic potential of blocking excessive mitochondrial fission in the treatment of human diseases.<sup>50</sup> In this research, we found that Tbx21 suppressed the mitochondrial fission and cell apoptosis. Intriguingly, the inhibition of MAPK/ERK signaling pathway weakened the inhibitory effect of Tbx21 on mitochondrial fission and cell apoptosis. Thus, we identified that Tbx21 modulates mitochondrial fission and cell apoptosis through MAPK/ERK signaling pathway.

## Conclusion

In conclusion, the present study demonstrated that miR-322-5p enhanced the apoptosis of AKI renal tubular epithelial cells via inhibiting Tbx21 expression. Additionally, we revealed that miR-322-5p activated MAPK/ERK signaling pathway to modulate the apoptosis of AKI mouse renal tubular epithelial cells. Further investigations will focus on other signals modified by miR-322-5p except Tbx21/MAPK/ERK axis in the future research.

## Authors' contributions

Li Fan: conception and design, administrative support.

Xiaodong Liu: collection and assembly of data, data analysis and interpretation.

Xiaobing Ji and Xiangxiang Li: collection and assembly of data, data analysis and interpretation.

Xin Du: collection and assembly of data, data analysis and interpretation.

Manuscript writing: all authors.

Final approval of manuscript: all authors.

## Statement of ethics

Animal study was approved by the Ethics Committee of the Nanjing First Hospital.

## Data availability statement

Not applicable.

## Funding sources

This research did not receive any specific grant from funding agencies in the public, commercial, or not-for-profit sectors.

## Conflict of interest

The authors have no conflicts of interest to declare.

## Acknowledgement

Thanks for all members.

## Appendix A. Supplementary data

Supplementary data associated with this article can be found, in the online version, at [doi:10.1016/j.nefro.2023.01.009](https://doi.org/10.1016/j.nefro.2023.01.009).

## REFERENCES

- Rahman M, Shad F, Smith MC. Acute kidney injury: a guide to diagnosis and management. *Am Fam Physician*. 2012;86:631–9.
- Fortrie G, de Geus HRH, Betjes MGH. The aftermath of acute kidney injury: a narrative review of long-term mortality and renal function. *Crit Care (Lond, Engl)*. 2019;23, <http://dx.doi.org/10.1186/s13054-019-2314-z>.
- Farrar A. Acute kidney injury. *Nurs Clin N Am*. 2018;53:499–510, <http://dx.doi.org/10.1016/j.cnur.2018.07.001>.
- Bellomo R, Kellum JA, Ronco C. Acute kidney injury. *Lancet (Lond, Engl)*. 2012;380:756–66, [http://dx.doi.org/10.1016/s0140-6736\(11\)61454-2](http://dx.doi.org/10.1016/s0140-6736(11)61454-2).
- Pu M, Chen J, Tao Z, Miao L, Qi X, Wang Y, et al. Regulatory network of miRNA on its target: coordination between transcriptional and post-transcriptional regulation of gene expression. *Cell Mol Life Sci*. 2019;76:441–51, <http://dx.doi.org/10.1007/s00018-018-2940-7>.
- Ledeganck KJ, Gielis EM, Abramowicz D, Stenvinkel P, Shiels PG, Van Craenenbroeck AH. MicroRNAs in AKI and kidney transplantation. *Clin J Am Soc Nephrol*. 2019;14:454–68, <http://dx.doi.org/10.2215/cjn.08020718>.
- Ren GL, Zhu J, Li J, Meng XM. Noncoding RNAs in acute kidney injury. *J Cell Physiol*. 2019;234:2266–76, <http://dx.doi.org/10.1002/jcp.27203>.
- Chen HH, Lan YF, Li HF, Cheng CF, Lai PF, Li WH, et al. Urinary miR-16 transactivated by C/EBPβ reduces kidney function after ischemia/reperfusion-induced injury. *Sci Rep*. 2016;6:27945, <http://dx.doi.org/10.1038/srep27945>.
- Lan YF, Chen HH, Lai PF, Cheng CF, Huang YT, Lee YC, et al. MicroRNA-494 reduces ATF3 expression and promotes AKI. *J Am Soc Nephrol*. 2012;23:2012–23, <http://dx.doi.org/10.1681/asn.2012050438>.
- Liu J, Hua R, Gong Z, Shang B, Huang Y, Guo L, et al. Human amniotic epithelial cells inhibit CD4+ T cell activation in acute kidney injury patients by influencing the miR-101-c-Rel-IL-2 pathway. *Mol Immunol*. 2017;81:76–84, <http://dx.doi.org/10.1016/j.molimm.2016.11.019>.
- Xu Y, Liu Z, Lv L, Li P, Xiu B, Qian W, et al. MiRNA-340-5p mediates the functional and infiltrative promotion of tumor-infiltrating CD8(+) T lymphocytes in human diffuse large B cell lymphoma. *J Exp Clin Cancer Res*. 2020;39:238, <http://dx.doi.org/10.1186/s13046-020-01752-2>.
- Zhu Z, Luo L, Xiang Q, Wang J, Liu Y, Deng Y, et al. MiRNA-671-5p promotes prostate cancer development and metastasis by targeting NFIA/CRYAB axis. *Cell Death Dis*. 2020;11:949, <http://dx.doi.org/10.1038/s41419-020-03138-w>.
- Ding C, Ding X, Zheng J, Wang B, Li Y, Xiang H, et al. miR-182-5p and miR-378a-3p regulate ferroptosis in I/R-induced renal injury. *Cell Death Dis*. 2020;11:929, <http://dx.doi.org/10.1038/s41419-020-03135-z>.
- Zhou G, Yang J, Song P. Correlation of ERK/MAPK signaling pathway with proliferation and apoptosis of colon cancer cells. *Oncol Lett*. 2019;17:2266–70, <http://dx.doi.org/10.3892/ol.2018.9857>.
- Xu WH, Zhang JB, Dang Z, Li X, Zhou T, Liu J, et al. Long non-coding RNA URHC regulates cell proliferation and apoptosis via ZAK through the ERK/MAPK signaling pathway

- in hepatocellular carcinoma. *Int J Biol Sci.* 2014;10:664–76, <http://dx.doi.org/10.7150/ijbs.8232>.
16. Zhang S, Li R, Dong W, Yang H, Zhang L, Chen, et al. RIPK3 mediates renal tubular epithelial cell apoptosis in endotoxin-induced acute kidney injury. *Mol Med Rep.* 2019;20:1613–20, <http://dx.doi.org/10.3892/mmr.2019.10416>.
  17. Li C, Wu J, Li Y, Xing G. Cytoprotective effect of heat shock protein 27 against lipopolysaccharide-induced apoptosis of renal epithelial HK-2 cells. *Cell Physiol Biochem.* 2017;41:2211–20, <http://dx.doi.org/10.1159/000475636>.
  18. Wang Z, Wu J, Hu Z, Luo C, Wang P, Zhang Y, et al. Dexmedetomidine alleviates lipopolysaccharide-induced acute kidney injury by inhibiting p75NTR-mediated oxidative stress and apoptosis. *Oxid Med Cell Longevity.* 2020, <http://dx.doi.org/10.1155/2020/5454210>, 5454210.
  19. Livak KJ, Schmittgen TD. Analysis of relative gene expression data using real-time quantitative PCR and the 2<sup>(-Delta Delta C(T))</sup> Method. *Methods (San Diego, Calif).* 2001;25:402–8, <http://dx.doi.org/10.1006/meth.2001.1262>.
  20. Wu X, Ding M, Liu Y, Xia X, Xu FL, Yao J, et al. hsa-miR-3177-5p and hsa-miR-3178 inhibit 5-HT1A expression by binding the 3'-UTR region in vitro. *Front Mol Neurosci.* 2019;12:13, <http://dx.doi.org/10.3389/fnmol.2019.00013>.
  21. Wang W, Zhu M, Xu Z, Li W, Dong X, Chen Y, et al. Ropivacaine promotes apoptosis of hepatocellular carcinoma cells through damaging mitochondria and activating caspase-3 activity. *Biol Res.* 2019;52:36, <http://dx.doi.org/10.1186/s40659-019-0242-7>.
  22. Jiang R, Chen X, Ge S, Wang Q, Liu Y, Chen H, et al. MiR-21-5p induces pyroptosis in colorectal cancer via TGFBI. *Front Oncol.* 2020;10:610545, <http://dx.doi.org/10.3389/fonc.2020.610545>.
  23. Fu Y, Zhang X, Liu X, Wang P, Chu W, Zhao W, et al. The DNMT1-PAS1-PH20 axis drives breast cancer growth and metastasis. *Signal Transduct Target Therapy.* 2022;7:81, <http://dx.doi.org/10.1038/s41392-022-00896-1>.
  24. Zhao N, Qin W, Wang D, Raquel AG, Yuan L, Mao Y, et al. MicroRNA-1 affects the development of the neural crest and craniofacial skeleton via the mitochondrial apoptosis pathway. *Exp Therap Med.* 2021;21:379, <http://dx.doi.org/10.3892/etm.2021.9810>.
  25. Lu HY, Wang GY, Zhao JW, Jiang HT. Knockdown of lncRNA MALAT1 ameliorates acute kidney injury by mediating the miR-204/APOL1 pathway. *J Clin Lab Anal.* 2021;35:e23881, <http://dx.doi.org/10.1002/jcla.23881>.
  26. Hui H, Ma W, Cui J, Gong M, Wang Y, Zhang Y, et al. Periodic acid-Schiff staining method for function detection of liver cells is affected by 2% horse serum in induction medium. *Mol Med Rep.* 2017;16:8062–8, <http://dx.doi.org/10.3892/mmr.2017.7587>.
  27. Liao JC, Chang WT, Lan YH, Hour MJ, Lee HZ. Application of proteomics to identify the target molecules involved in *Lonicera japonica*-induced photokilling in human lung cancer CH27 cells. *BMC Complement Alternat Med.* 2013;13:244, <http://dx.doi.org/10.1186/1472-6882-13-244>.
  28. Tao M, Shi Y, Tang L, Wang Y, Fang L, Jiang W, et al. Blockade of ERK1/2 by U0126 alleviates uric acid-induced EMT and tubular cell injury in rats with hyperuricemic nephropathy. *Am J Physiol Renal Physiol.* 2019;316:F660–73, <http://dx.doi.org/10.1152/ajprenal.00480.2018>.
  29. Correia de Sousa M, Gjorgjieva M, Dolicka D, Sobolewski C, Foti M. Deciphering miRNAs' action through miRNA editing. *Int J Mol Sci.* 2019;20, <http://dx.doi.org/10.3390/ijms20246249>.
  30. Wang X, Lu X, Zhang T, Wen C, Shi M, Tang X, et al. mir-329 restricts tumor growth by targeting grb2 in pancreatic cancer. *Oncotarget.* 2016;7:21441–53, <http://dx.doi.org/10.18632/oncotarget.7375>.
  31. Qin B, Shu Y, Long L, Li H, Men X, Feng L, et al. MicroRNA-142-3p induces atherosclerosis-associated endothelial cell apoptosis by directly targeting rictor. *Cell Physiol Biochem.* 2018;47:1589–603, <http://dx.doi.org/10.1159/000490932>.
  32. Eleftheriadis T, Sounidaki M, Pissas G, Antoniadis G, Liakopoulos V, Stefanidis I. In human alloreactive CD4+ T-cells, dichloroacetate inhibits aerobic glycolysis, induces apoptosis and favors differentiation towards the regulatory T-cell subset instead of effector T-cell subsets. *Mol Med Rep.* 2016;13:3370–6, <http://dx.doi.org/10.3892/mmr.2016.4912>.
  33. Che Q, Wang W, Duan P, Fang F, Liu C, Zhou T, et al. Downregulation of miR-322 promotes apoptosis of GC-2 cell by targeting Ddx3x. *Reprod Biol Endocrinol.* 2019;17:63, <http://dx.doi.org/10.1186/s12958-019-0506-7>.
  34. Weng C, Chen Y, Wu Y, Liu X, Mao H, Fang X, et al. Silencing UBE4B induces nasopharyngeal carcinoma apoptosis through the activation of caspase3 and p53. *Oncotargets Therapy.* 2019;12:2553–61, <http://dx.doi.org/10.2147/ott.S196132>.
  35. Zhan S, Wang C, Yin F. MicroRNA-29c inhibits proliferation and promotes apoptosis in non-small cell lung cancer cells by targeting VEGFA. *Mol Med Rep.* 2018;17:6705–10, <http://dx.doi.org/10.3892/mmr.2018.8678>.
  36. Karbowski M, Lee YJ, Gaume B, Jeong SY, Frank S, Nechushtan A, et al. Spatial and temporal association of Bax with mitochondrial fission sites, Drp1, and Mfn2 during apoptosis. *J Cell Biol.* 2002;159:931–8, <http://dx.doi.org/10.1083/jcb.200209124>.
  37. Qian J, Fang D, Lu H, Cao Y, Zhang J, Ding R, et al. Tanshinone IIA promotes IL2-mediated SW480 colorectal cancer cell apoptosis by triggering INF2-related mitochondrial fission and activating the Mst1-Hippo pathway. *Biomed Pharmacotherapy.* 2018;108:1658–69, <http://dx.doi.org/10.1016/j.biopha.2018.09.170>.
  38. Jiang W, Xu J, Shen B, Wang Y, Teng J, Ding X. Acute kidney injury risk assessment. *Contrib Nephrol.* 2018;193:13–20, <http://dx.doi.org/10.1159/000484959>.
  39. Jones TF, Bekele S, O'Dwyer MJ, Prowle JR. MicroRNAs in acute kidney injury. *Nephron.* 2018;140:124–8, <http://dx.doi.org/10.1159/000490204>.
  40. Wei Q, Sun H, Song S, Liu Y, Liu P, Livingston MJ, et al. MicroRNA-668 represses MTP18 to preserve mitochondrial dynamics in ischemic acute kidney injury. *J Clin Investig.* 2018;128:5448–64, <http://dx.doi.org/10.1172/jci121859>.
  41. Zhu X, Li W, Li H. miR-214 ameliorates acute kidney injury via targeting DKK3 and activating of Wnt/ $\beta$ -catenin signaling pathway. *Biol Res.* 2018;51:31, <http://dx.doi.org/10.1186/s40659-018-0179-2>.
  42. Valinezhad Orang A, Safaralizadeh R, Kazemzadeh-Bavili M. Mechanisms of miRNA-mediated gene regulation from common downregulation to mRNA-specific upregulation. *Int J Genomics.* 2014, <http://dx.doi.org/10.1155/2014/970607>, 970607.
  43. Zeng Y, Du C, Xiao P, Lei Y, Zhao P, Zhu Z, et al. Sox9-increased miR-322-5p facilitates BMP2-induced chondrogenic differentiation by targeting Smad7 in mesenchymal stem cells. *Stem Cells Int.* 2021, <http://dx.doi.org/10.1155/2021/9778207>, 9778207.
  44. Connolly M, Garfield BE, Crosby A, Morrell NW, Wort SJ, Kemp PR. miR-322-5p targets IGF-1 and is suppressed in the heart of rats with pulmonary hypertension. *FEBS Open Bio.* 2018;8:339–48, <http://dx.doi.org/10.1002/2211-5463.12369>.
  45. Zheng W, Zhang J, Zhou B, Chang H. MiR-322-5p alleviates cell injury and impairment of cognitive function in vascular dementia by targeting TSPAN5. *Yonsei Med J.* 2022;63:282–91, <http://dx.doi.org/10.3349/yymj.2022.63.3.282>.
  46. Wang N, Li Y, Wei J, Pu J, Liu R, Yang Q, et al. TBX1 functions as a tumor suppressor in thyroid cancer through inhibiting the

- activities of the PI3K/AKT and MAPK/ERK pathways. *Thyroid*. 2019;29:378–94, <http://dx.doi.org/10.1089/thy.2018.0312>.
47. Tao L, Zhang CY, Guo L, Li X, Han NN, Zhou Q, et al. MicroRNA-497 accelerates apoptosis while inhibiting proliferation, migration, and invasion through negative regulation of the MAPK/ERK signaling pathway via RAF-1. *J Cell Physiol*. 2018;233:6578–88, <http://dx.doi.org/10.1002/jcp.2018.26272>.
48. Tilokani L, Nagashima S, Paupe V, Prudent J. Mitochondrial dynamics: overview of molecular mechanisms. *Essays Biochem*. 2018;62:341–60, <http://dx.doi.org/10.1042/ebc20170104>.
49. Elgass K, Pakay J, Ryan MT, Palmer CS. Recent advances into the understanding of mitochondrial fission. *Biochim Biophys Acta*. 2013;1833:150–61, <http://dx.doi.org/10.1016/j.bbamcr.2012.05.002>.
50. Serasinghe MN, Chipuk JE. Mitochondrial fission in human diseases. *Handbook Exp Pharmacol*. 2017;240:159–88, [http://dx.doi.org/10.1007/164\\_2016\\_38](http://dx.doi.org/10.1007/164_2016_38).